J Mol Model (2011) 17:3219–3228
DOI 10.1007/s00894-011-0996-5

ORIGINAL PAPER

Atomistic modeling of parylene-metal interactions for surface micro-structuring

Alex V. Vasenkov

Received: 16 November 2010 / Accepted: 26 January 2011 / Published online: 3 March 2011
© Springer-Verlag 2011

Abstract Many applications, ranging from neural prosthetics and cardiac rhythm management systems to organics-based flexible display, can benefit from the engineering of parylene-metal-parylene structures via selective deposition. Despite several experimental studies, the mechanism responsible for this selective deposition is not clear and is the subject of the current paper. Towards this goal, we used the quantum semiempirical Hamiltonian (QSH) solver coupled to a molecular dynamic (MD) model, which is particularly suited to study parylene-metal interactions due to its ability to determine the different pathways of the transformations involving making and breaking of chemical and physical bonds. The simulation results of selective deposition of various parylene chains on titanium dioxide and gold surfaces are presented. Time-dependent bond orders were used to quantify the deposition process. The mechanism of metal atom adhesion to parylene was also discussed to provide insights into the formation of defects in metal/parylene interfaces.

Keywords Atomistic modeling · Parylene-metal interactions · Surface micro-structuring

Introduction

Fabrication of microstructured electrode surfaces is of great interest to many applications, ranging from neural prosthetics [1, 2] and cardiac rhythm management systems [3] to organics-based flexible display [4]. Most of these applications require the engineering of isolated micro-sized islands of conformal polymer coating on electrode surfaces. Conventional methods of fabrication of such islands involve photolithography process. Unfortunately, this process requires the use of solvents and acids, resulting in polymer surface defect formation via undesirable chemical side reactions. One way of avoiding photolithography is the patterning of an electrode via controlled deposition of conformal polymer coatings [3, 5]. Parylene and its derivatives have showed great promise in enabling selective deposition of such a conformal coating. For example, selective inhibition of both non-reactive parylene coatings [6, 7] as well as reactive parylene coatings [8] have been reported.

Despite several experimental studies [6–8], the mechanism of parylene-metal interactions responsible for the observed selective inhabitation is not clear and is the subject of the current paper. Towards this goal, we use molecular dynamic (MD) methods, which are particularly suited to study parylene-metal interactions due to the ability to determine the different pathways of transformations involving the making and breaking of chemical and physical bonds. Force fields (interatomic potentials) play a critical role in MD modeling. Classical MD models with empirical reactive force fields are suitable for modeling polymers [9], but are too simple to predict complex polymer–metal interactions. Ideally, high level ab initio molecular-orbital or density-functional calculations should be used in computing force fields to eliminate any need for parameters. The primary drawback of such an approach is the large amount of computational time required, which limits the MD method to studying small clusters only. In this work, we used the quantum semiempirical Hamiltonian (QSH) solver coupled to the MD model to gain insight into

A. V. Vasenkov (✉)
CFD Research Corporation,
215 Wynn Drive,
Huntsville, AL 35805, USA
e-mail: avv@cfdrc.com

the physical adsorption and chemical reactions that occur during metal/polymer interface formation.

The advantage of our method is its ability to model breaking and making bonds within the quantum chemical framework orders of magnitude faster than with ab initio methods. QSH-MD offers a compromise between high-level quantum description and computational speed. Over the past 50 years, QSH techniques have been developed extensively as computationally more efficient alternatives to ab initio methods [10]. PM6-QSH [10] parameterization implemented in MOPAC 7.2 was used in this work for the accurate modeling of polymer/metal interactions. The paper is arranged as follows. First, we briefly describe the QSH-MD model used to model elementary reaction pathways on a complex potential energy surface at a finite temperature. Then, the QSH-MD simulation results of deposition of commercial chloro-p-xylylene and dichloro-p-xylylene, and functionalized (reactive) vinyl-p-xylylene on gold (Au) and titanium dioxide (TiO_2) surfaces are presented. Time-dependent bond orders were used to quantify the deposition process. Finally, the mechanism of adhesion of bio-compatible platinum (Pt) and iridium (Ir) metals as well as adhesion of the promoter titanium (Ti) to parylene-C and Parylene-HT chains are discussed to provide insight into the formation of defects in metal/parylene interfaces.

Models

Coupled QSH-MD modeling

In this section we outline the model used for modeling elementary reaction pathways on a complex potential energy surface at a finite temperature. This model couples classical MD simulation with QSH modeling. The details of the model have been described previously [11, 12], so only a brief outline is given here.

QSH-MD coupling

Existing QSH models typically are either not capable of computing gradients for periodic systems or do it extremely slowly [13]. To address this problem, we used two groups of atoms in our MD simulations: empirical atoms located at the bottom and sides, and quantum atoms forming a cluster surrounded by empirical atoms. Interactions between empirical atoms, and between empirical atoms and quantum cluster were simulated using empirical (analytical) Morse potential [14]. Forces acting on quantum atoms were modeled based on a molecular-cluster QSH approach as detailed below. The quantum atoms were used to model physical adsorption and chemical reactions, while empirical atoms were used to eliminate side effects.

At the end of each dynamic step in the MD module, coordinates of atoms constituting a quantum cluster were saturated with hydrogen atoms and transferred to the QSH module. Instantaneous potential energy and interatomic forces were computed in the QSH module and fed back to the MD module. Here, the contributions from the ghost hydrogen atoms were zeroed, and forces acting on quantum atoms were combined with the Morse-type forces computed for empirical atoms. In the first iteration between MD and QSH modules, a default guess of molecular orbital coefficients was used. At subsequent iterations, the set of molecular orbital coefficients describing the electronic structure at the previous time step was used to reduce the time needed to reach self consistent field (SCF). At the end of iterations in the QSH module, bond orders, charge densities, and other quantum mechanics properties were calculated from the density matrix elements. This information was used in the visualization of chemical reactions and surface motion.

MD module

The MD module is based on a numerical solution of the many-body problem of classical mechanics. For an isolated system containing a constant number of atoms N in a fixed volume V, the atomic motion is given by Newton's equations,

$$\vec{F}_i(t) = m\frac{d^2\vec{r}_i}{dt^2} = -\frac{\partial U(\vec{r}_1, \vec{r}_2, ...\vec{r}_N)}{\partial \vec{r}_i}, \quad (1)$$

Where $\vec{F}_i$ is the force acting on atom i caused by the N−1 other atoms and U is the potential energy depending on the positions of atoms in the system. Iteratively integrating Eq. 1, one can obtain trajectories of each atom. Beeman's third-order predictor algorithm was used to integrate Newton's equations of motion. This algorithm is written as [15]

$$\vec{r}_{n+1} = \vec{r}_n + \vec{v}_{n+1}\Delta t + \frac{1}{6}(4\vec{a}_n - \vec{a}_{n-1})(\Delta t)^2 \quad (2)$$

$$\vec{v}_{n+1} = \vec{v}_n + \frac{1}{6}(2\vec{a}_{n+1} + 5\vec{a}_n - \vec{a}_{n-1})(\Delta t) \quad (3)$$

where $\vec{r}_n$, is the position, $\vec{v}_n$ is the velocity, $\vec{a}_n$ is the acceleration on the n-th time step, and Δt is the duration of time step. A time step of 0.5 fs was typically used in MD computations to maintain stable dynamics.

Effective temperature control in MD simulations was achieved using the Berendsen thermostat method. In this method, atomic velocities are scaled after each dynamic time step by a factor η given by [16]

$$\eta = \left[1 + \frac{\Delta t}{\tau}\left(\frac{T_o}{T} - 1\right)\right]^{1/2} \quad (4)$$

where τ is an adjustable parameter, T_o is the desired temperature to be maintained, and T is the instantaneous temperature of the system.

Construction of surface models

The models of Au and TiO_2 surfaces were constructed by truncating an infinite crystal lattice of interest to a size that is computationally tractable. Figure 1 shows truncation of Au face-centered cubic crystal lattice schematically [17]. The surface model of (110) TiO_2 adopted from [18] is given in Fig. 2. Boundary ghost atoms were added to eliminate bottom- and side-surface effects. In QSH calculations, the boundaries of clusters consisting of quantum atoms were saturated with "ghost" hydrogen atoms as shown in Fig. 2. The distance between the ghost hydrogen atoms, and the quantum cluster was determined by scaling distances between quantum and empirical boundary atoms.

The MOPAC 7.2 quantum chemical package with parameterization accounting for d orbitals was used to compute interatomic potentials due to its ability to model interactions with transition metal atoms [10]. The lowest electronic state of the quantum cluster was determined

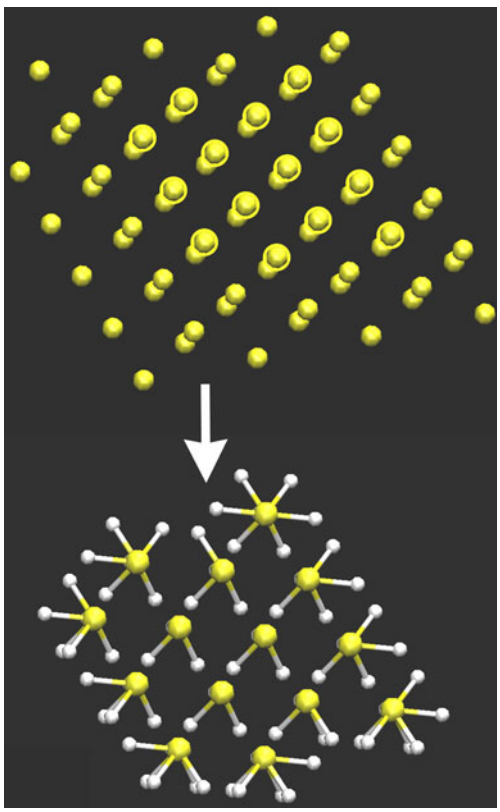

Fig. 1 Schematic demonstrating the truncation of Au face-centered cubic crystal lattice to a computationally tractable surface model. Quantum Au atoms (*yellow spheres*) were passivated with hydrogen atoms (*white spheres*) for computing quantum semiempirical Hamiltonian (QSH) potential. See text for details

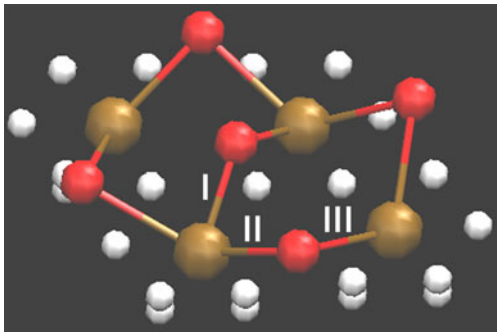

Fig. 2 Surface models of titanium dioxide. Quantum Ti atoms (*brown spheres*) were passivated with hydrogen atoms (*white spheres*) for computing QSH potential. See text for details

using the PM6 semi-empirical SCF methods of the MOPAC 7.2 software. PM6 parameterization was developed to match experimental heat of formation rather than bond energies. Therefore, we tested both unrestricted Hartree–Fock (UHF) and configuration interaction (CI) methods for bond energy and bond length, and determined that CI typically gives better accuracy. This is due to the presence of degenerate d-orbitals where single configuration is an inaccurate description of the wave function [10]. Consequently, the CI method was used to obtain the simulation results presented in this paper.

Au–Au interactions are difficult to describe as they result from electron correlation of the closed-shell components, somewhat similar to van der Waals interactions but unusually strong due to relativistic effects [17, 19]. We found that PM6 Hamiltonian gives an Au–Au bond energy of 8.1 kcal mol^{-1} and a bond length of 2.8 Å. These results are in very good agreement with the literature bond energy of 7–12 kcal mol^{-1} and bond length of 2.7–3.3 Å [17, 19, 20]. The bond order, which gives an indication of the stability of the Au–Au bond, was 0.06 due to the weak Au–Au interactions. We also tested the use of PM6 Hamiltonian for predicting TiO_2 crystal lattice. Bond lengths between the different pairs of Ti and O atoms obtained using PM6-QSH are compared with the literature data in Table 1. We found that the ratios of experimental Ti–O bond lengths were reproduced qualitatively by the PM6 QSH model, but the absolute PM6 Ti–O bond lengths typically over-estimate experimental and ab initio data as previously discussed [10, 21].

Computational details

QSH-MD simulations were conducted using an AMD-64 Opteron 2600 MHz computer system. The duration of QSH-MD jobs depended strongly on the number of quantum atoms, and varied from 48 to 240 CPU hours. The number of quantum atoms used in the QSH module varied from 50 atoms for metal–parylene adhesion simulations to over 100 atoms for modeling the deposition of poly-p-xylylenes on metal

Table 1 Relaxed bond lengths for selected Ti–O atom pairs in the TiO2 (110) surface model. Results from the MOPAC 7.2 PM6 Hamiltonian [10] used in this study are compared with literature data

Bond label	Bond length (Å)			
	Experimental (1997) [29]	Experimental (2005) [30]	Ab initio [18]	Present 7.2 MOPAC
I	1.71±0.07	1.85	1.84	1.97
II	2.15±0.09	2.15	2.04	2.28
III	1.84±0.05	1.90	1.92	2.22

surfaces. The MOPAC 7.2-QSH model often has convergence issues if the number of atoms exceeds 150.

Selective deposition of poly-p-xylylenes on metals

The contrasting deposition of poly-p-xylylenes on titanium and gold—two popular metals used in the fabrication of implantable electrodes [2]—was determined. For this purpose, we considered commercial chloro-p-xylylene and dichloro-p-xylylene as well as functionalized (reactive) vinyl-p-xylylene [8]. The structure of selected poly-p-xylylenes is presented in Fig. 3. A poly-p-xylylene was placed 5–6 Å above the metal surface with thermal velocity pointed toward the surface. The geometry of the metal surface consisting of quantum atoms and empirical atoms, introducing boundary potential at the side walls, was optimized by minimizing its potential energy. Our QSH-MD model is very efficient in determining the minimum potential energy configuration via a dynamic quenching procedure [11]. In this procedure, the velocities of individual atoms were monitored and reset to zero when they had reached a maximum value. The high efficiency of the procedure is due to the inverse relationship between kinetic and potential energies. When the velocity of an atom is large, its potential energy must be small. After the energy minimization procedure, the metal surface was equilibrated at 300 K. Initial interactions between a poly-p-xylylene and a metal surface were weak as tested by computing a bond order. Typically, the initial bond order was below 10^{-3}.

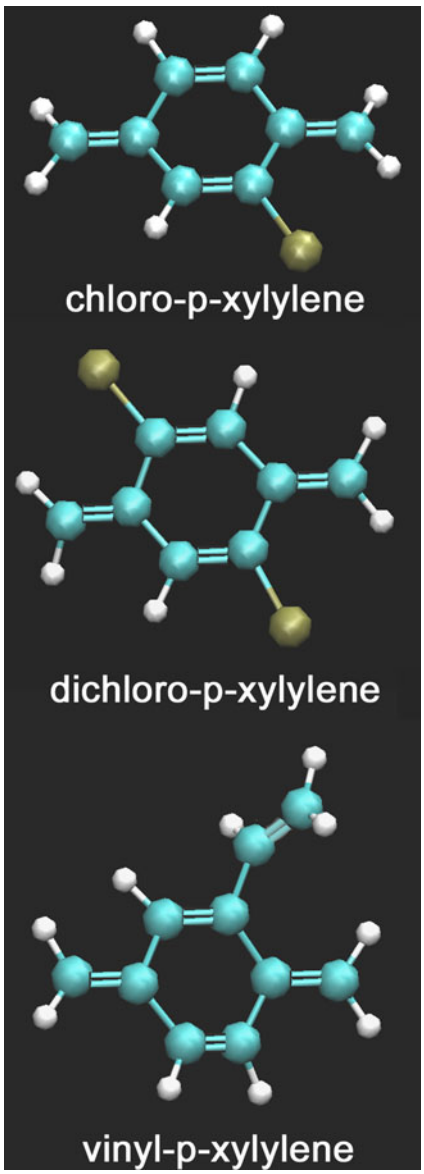

Fig. 3 Nonfunctionalized chloro-p-xylylene and dichloro-p-xylylene, and functionalized (reactive) vinyl-p-xylylene were considered to study selective deposition. Cl, C, and H atoms are represented by *tan*, *cyan*, and *white spheres*, respectively

Chloro-p-xylylene deposition

The deposition of chloro-p-xylylene on TiO_2 and Au surfaces is visualized in Fig. 4. Comparing the results at 0 and 0.25 ps shows that the shape of chloro-p-xylylene was affected substantially by interactions with the TiO_2 surface. In contrast, in the case of the Au surface, the chloro-p-xylylene shape evolved weakly from the initial configuration. A polar bond was formed between chloro-p-xylylene and the Au surface at 0.5 ps, and between chloro-p-xylylene and TiO_2 at 0.75 ps. Chloro-p-xylylene bonds preferentially to O atoms rather than to Ti atoms due to the

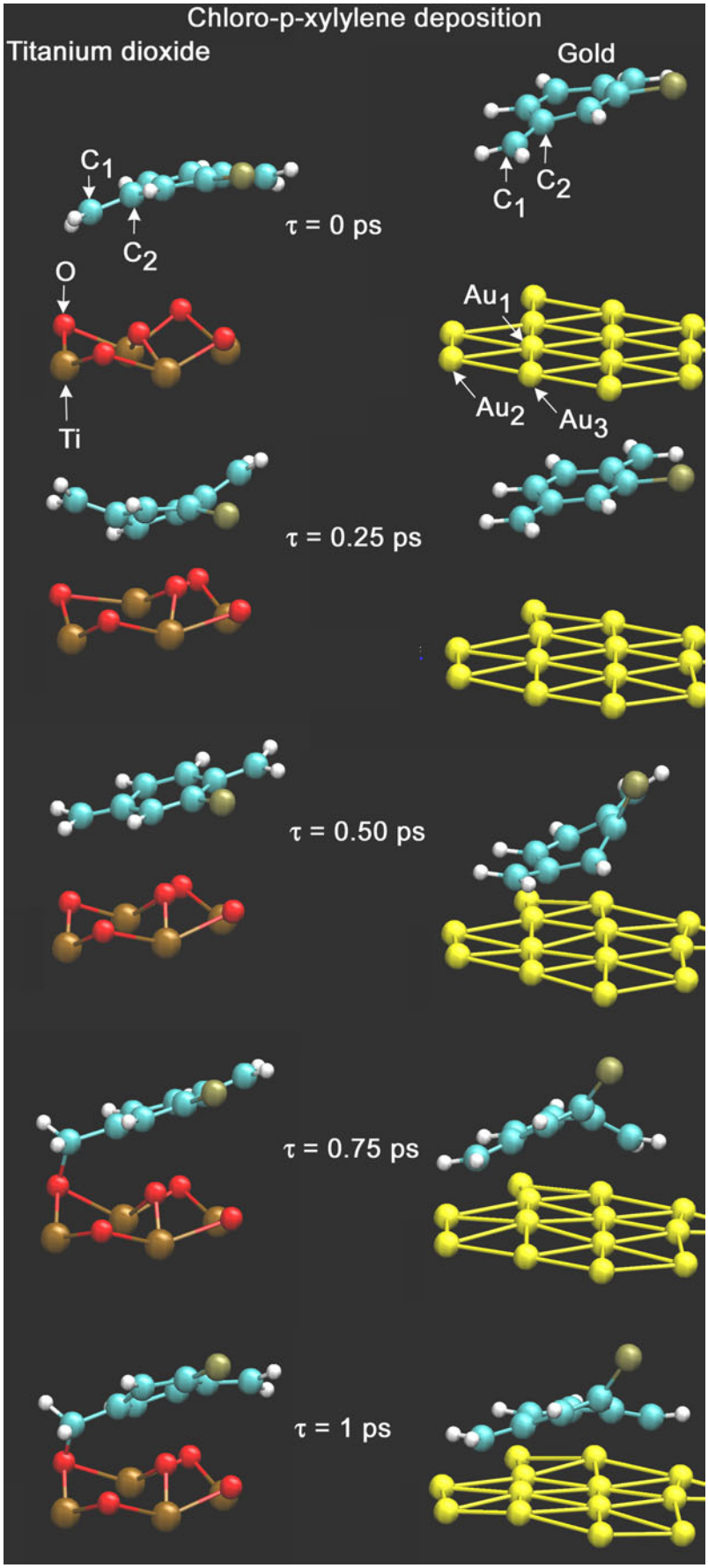

Fig. 4 Deposition of chloro-p-xylylene on titanium dioxide (TiO_2) and gold (Au)

higher electronegativity of O. Results at 1 ps confirm the completion of chloro-p-xylylene deposition. The stability of the bonds established was checked further via calculations of a few picoseconds in duration.

Quantitative description of the deposition process can be obtained by analyzing time-dependent profiles of bond orders, as presented in Fig. 5. In the case of the TiO_2 surface, the initial bond order between C_1–C_2 atoms was slightly less than 2.0 due to the strain resulting from the presence of the TiO_2 surface. The formation of the bond between chloro-p-xylylene and the TiO_2 surface at about 0.6 ps was accompanied by further weakening of the C_1–C_2 bond. The C_1–O bond formed was strong, with the bond order close to 1. The order of the C_1 –Ti bond was below 0.2 due to the weak C–Ti interaction. In the case of the Au surface, the bond order between C_1–C_2 atoms decreased from 1.9 to 1.6 during the deposition, indicating that the structure of chloro-p-xylylene was affected by interactions with the Au surface. The simulation results indicate that chloro-p-xylylene bonds preferentially to a solid Au trimer.

Dichloro-p-xylylene deposition

The deposition of dichloro-p-xylylene on TiO_2 and Au surfaces is shown in Fig. 6. In the case of the TiO_2 surface,

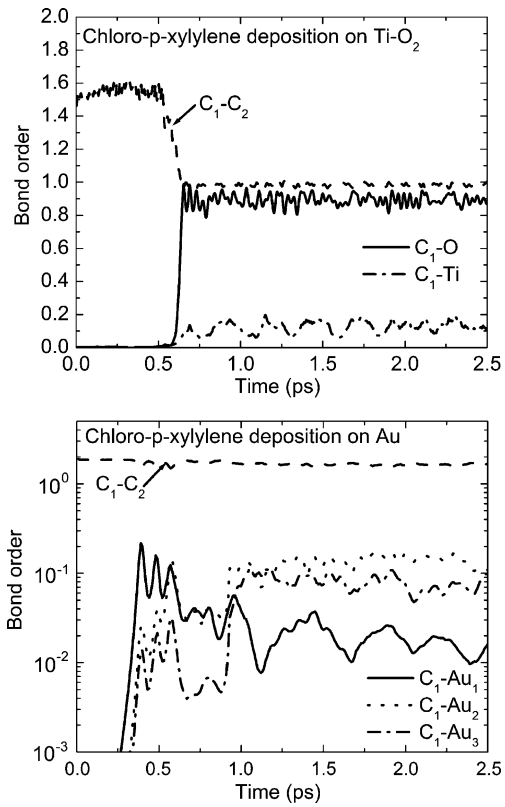

Fig. 5 Time-dependent profiles of bond orders during the deposition of chloro-p-xylylene on TiO_2 and Au. Designations for atoms are given in Fig. 4

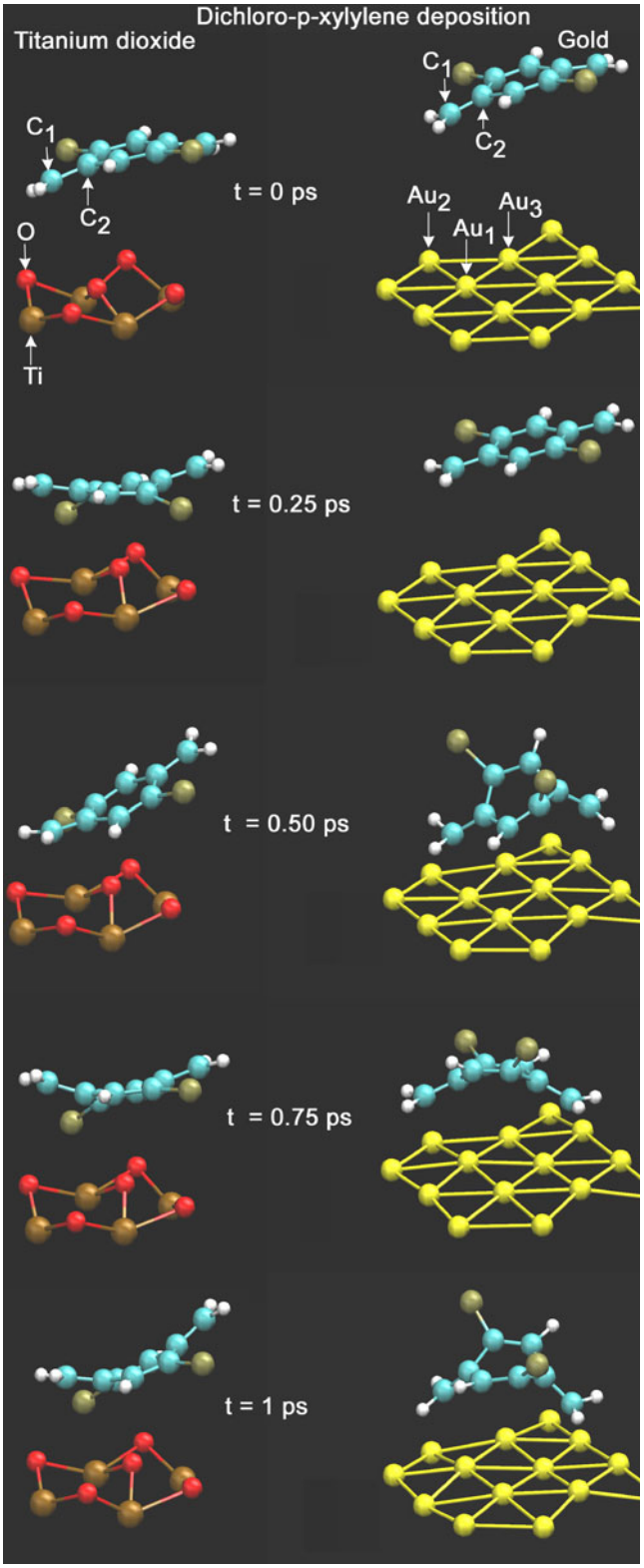

Fig. 6 Deposition of dichloro-p-xylylene on TiO_2 and Au

the shape of dichloro-p-xylylene is visibly distorted by interaction with the TiO_2 surface. However, in contrast to the deposition of chloro-p-xylylene, no bond formation between dichloro-p-xylylene and the TiO_2 surface was

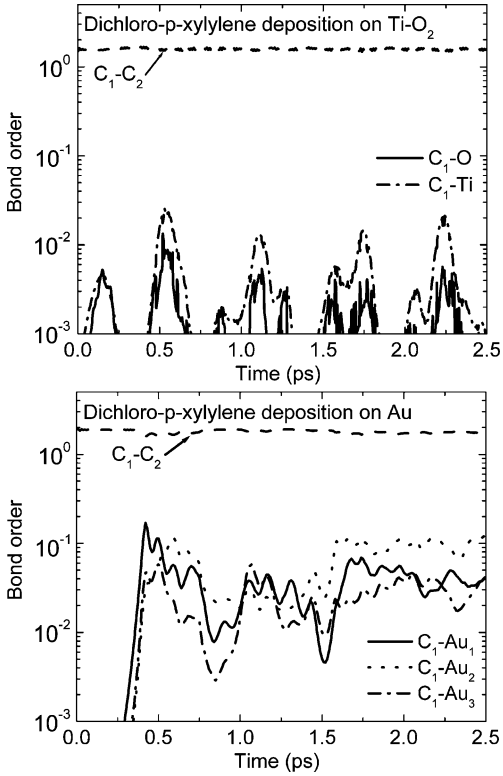

Fig. 7 Time-dependent profiles of bond orders during the deposition of dichloro-p-xylylene on TiO_2 and Au. Designations for atoms are given in Fig. 6

observed. This is due to the higher electronegativity of dichloro-p-xylylene owing to Cl substitution of H [22]. In the case of the Au surface, dichloro-p-xylylene formed stable bonds at about 0.5 ps.

Time-dependent profiles of bond orders during the metal–dichloro-p-xylylene interactions are given in Fig. 7. In the case of the TiO_2 surface, the order of the C_1–C_2 bond fluctuates near 1.6 due to the strains resulting from the TiO_2 surface. The orders of C_1–O and C_1–Ti bonds are below 0.03. In the case of the Au surface, the formation of bonds between dichloro-p-xylylene and the solid Au trimer was observed.

Vinyl-p-xylylene deposition

The deposition of vinyl-p-xylylene on TiO_2 and Au surfaces is shown in Fig. 8. In the case of the TiO_2 surface, vinyl-p-xylylene did not approach the surface indicating the lack of adsorption. In the case of the Au surface, vinyl-p-xylylene bonded to the surface at about 0.5 ps. Time-dependent profiles of bond orders are given in Fig. 9. In the case of the TiO_2 surface, the order of C_1–C_2 bond fluctuates at 1.7, while the orders of C_1–O and C_1–Ti bonds are below 3×10^{-4} due to the weak interactions with the TiO_2 surface. In the case of the Au surface, the formation of bonds

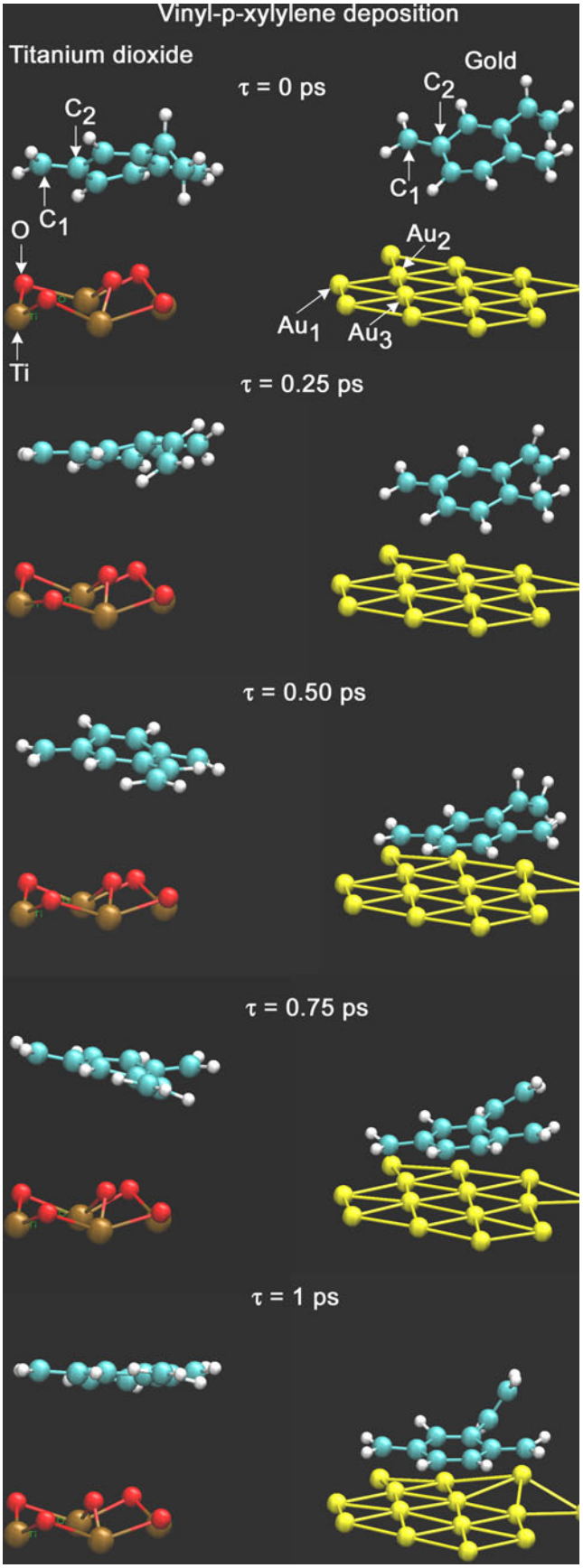

Fig. 8 Deposition of vinyl-p-xylylene on TiO_2 and Au ▶

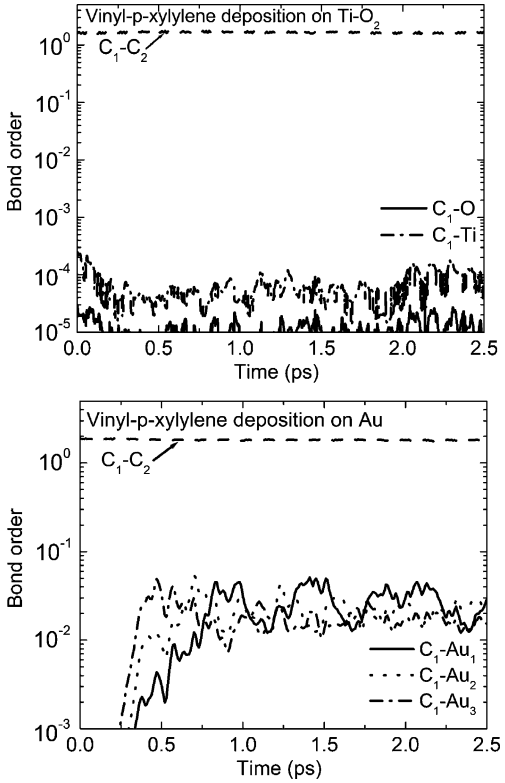

Fig. 9 Time-dependent profiles of bond orders during the deposition of vinyl-p-xylylene on TiO_2 and Au. Designations for atoms are given in Fig. 8

between vinyl-p-xylylene and the solid Au trimer was observed in a manner similar to that discussed for chloro-p-xylylene and dichloro-p-xylylene.

The absence of bond formation between vinyl-p-xylylene and the TiO_2 surface is due to the electronegativity of the vinyl group, whose value can be estimated by $E_g = \frac{V_c E_c + \sum_n N_n E_n}{N}$ [23]. Here, V_c and E_c are the valence of the central atom and its atomic electronegativity, respectively. N_n and E_n are the number of bonds towards the central atom and the electronegativity of the n-th atom (group), respectively. N is the sum of the valence of the central atom and the number of bonds towards the central atom. The estimated electronegativity of the vinyl group is 2.45, which is lower than the electronegativity of Cl in chloro-p-xylylene. Based on this consideration, and the results of chloro-p-xylylene–TiO_2 interactions presented in Figs. 4 and 5, one would expect that vinyl-p-xylylene should form a bond with TiO_2. However, the results presented in Fig. 8 and Fig. 9 contradict this conclusion. This disagreement can be explained as follows. The C–Cl bond in chloro-p-xylylene is a highly polar bond [22]. As a result of this, TiO_2 is capable of forming a CO bond with chloro-p-xylylene only when the highly electronegative Cl atom remains distant from the surface, as shown in Fig. 4. In contrast, vinyl-p-xylylene does not have a strong polar bond. In addition, the estimated electronegativity of the vinyl group of 2.45 is higher than the electronegativity of H of 2.20, which is substituted by the vinyl group to form vinyl-p-xylylene. This explains the absence of adsorption of vinyl-p-xylylene on TiO_2.

Selective adhesion of metal atoms to parylene

Lack of adhesion of metal atoms to a parylene surface is known to be responsible for the formation of defects in metal/parylene interfaces (W. Li, personal communication). To gain insight into metal/parylene adhesion, we considered the deposition of Ir and Pt on parylene-C and parylene-HT polymer chains. Ir and Pt are often used in implants due to their outstanding bio-compatible properties [24]. Time-dependent profiles of bond orders during the deposition of Pt and Ir on parylene-C (top panel) and parylene-HT (bottom panel) polymer chains are shown in Fig. 10. It was observed that Ir, with a lower electronegativity of 2.2, can form only a temporary bond with poly-p-xylylenes. In contrast, Pt, with a higher electronegativity of 2.3, can form

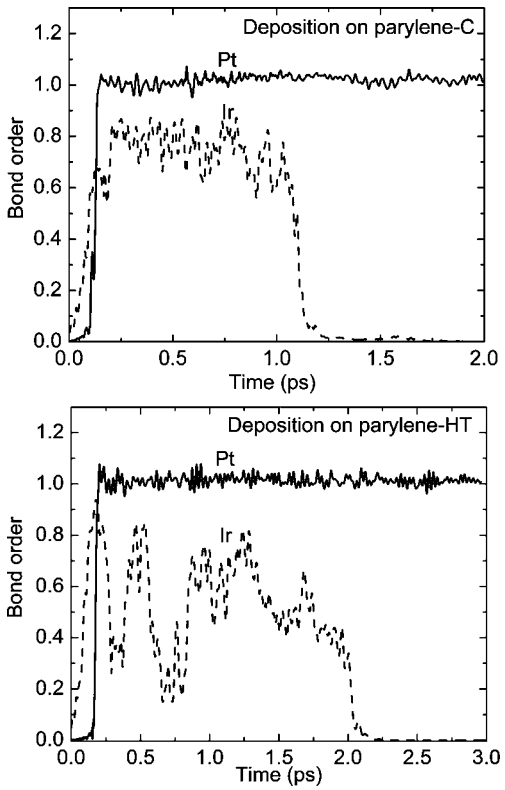

Fig. 10 Time-dependent profiles of bond orders during the deposition of Pt and Ir on parylene-C (*top panel*) and parylene-HT (*bottom panel*) polymer chains

a stable bond with both parylene-C and parylene-HT substrates.

The adhesion of Pt, and especially Ir, to parylene can be improved by introducing a promoter between parylene and a biocompatible metal such as Ti. To illustrate this, we conducted QSH-MD modeling of Ti deposition on parylene-C and parylene-HT polymer chains. In both cases, the formation of a strong C=Ti double bond was observed, as shown in Figs. 11 and 12. This is an agreement with the DFT bonding analysis reported in [25]. In contrast to the deposition of Pt and Ir, the deposition of Ti was accompanied by reactions. For example, in the case of parylene-C, a transition metal-catalyzed hydrogen transfer reaction was detected. Time dependent Ti–H_1 and Ti–H_2 bond orders are shown in Fig. 11. The ability of Ti to extract hydrogen from chemical compounds consisting of carbon and hydrogen is detailed in the literature [26, 27]. In the case of parylene-HT, Ti–C bond formation was accompanied by C–F bond breaking and Ti–F bond formation. These finding are in agreement with the fundamental principles of C–F bond activation and breaking mediated by transition metal centers as discussed previously [28].

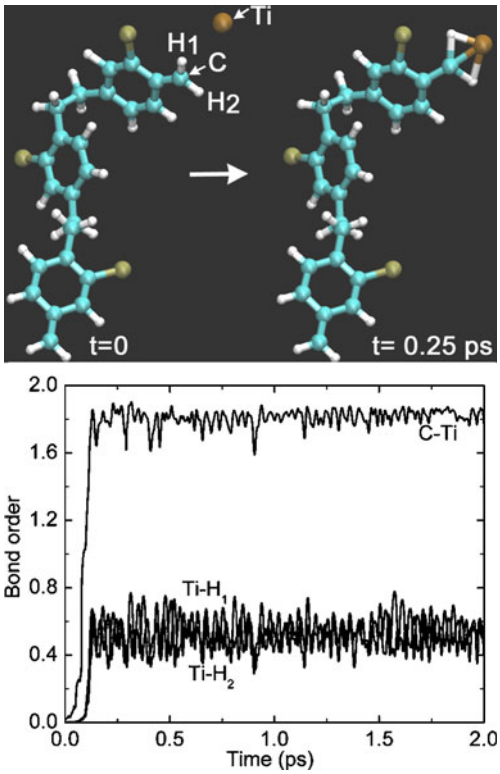

Fig. 11 Time-dependent profiles of bond orders during the deposition of Pt and Ir on parylene-C (top panel) and parylene-HT (bottom panel) polymer chains

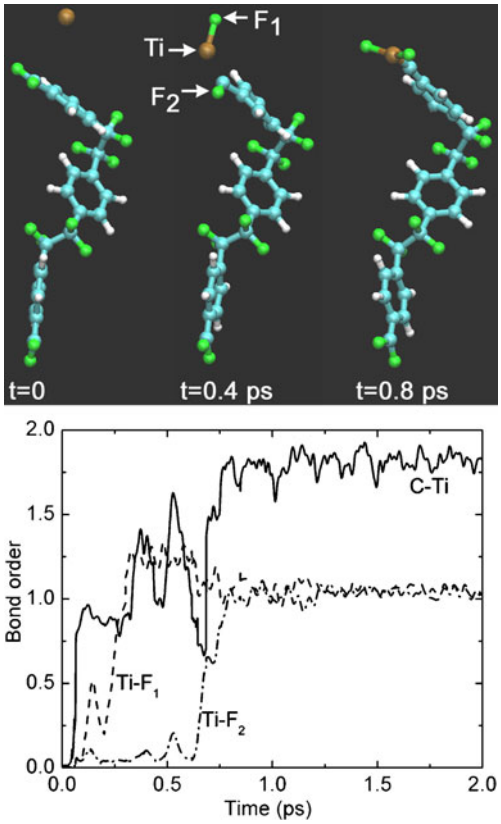

Fig. 12 QSH-molecular dymanics (MD) results demonstrating the deposition of Ti on a parylene-HT polymer chain

Summary

To gain insight into surface microstructuring, parylene–metal interactions were studied via MD simulations in conjunction with QSH modeling. The advantage of model is its ability to trace breaking and making chemical and physical bonds in real time within the quantum chemical framework, orders of magnitude faster than ab initio models. The selectivity of deposition of various poly-p-xylylenes on TiO_2 surfaces was demonstrated. The absence of bond formation of dichloro-p-xylylene or vinyl-p-xylylene with TiO_2 surfaces was explained in terms of electrostatic repulsion. In contrast, the formation of stable bonds between poly-p-xylylenes and solid Au trimers was observed in all cases.

Mechanisms of metal atom adhesion on parylene surfaces were also studied since these have been linked to the formation of defects in metal/parylene interfaces. Good adhesion of Pt, and poor adhesion of Ir to parylene was attributed to the lower electronegativity of Ir. It was demonstrated that Ti, often introduced as a promoter between parylene and a biocompatible metal, is capable of forming strong C=Ti double bonds.

References

1. HajjHassan M, Chodavarapu V, Musallam S (2008) NeuroMEMS: neural probe microtechnologies. Sensors 8:6704–6726. doi:10.3390/s8106704
2. Rodger DC, Fong AJ, Li W, Ameri H, Ahuja AK, Gutierrez C, Lavrov I, Zhong H, Menon PR, Meng E, Burdick JW, Roy RR, Edgerton VR, Weiland JD, Humayun MS, Tai YC (2008) Flexible parylene-based multielectrode array technology for high-density neural stimulation and recording. Sens Actuators B 132:449–460. doi:10.1016/j.snb.2007.10.069
3. Lobodzinski SS, Laks M (2009) New material for implantable cardiac leads. J Electrocard 42:566–573. doi:10.1016/j.jelectrocard.2009.07.019
4. Choia MC, Kimb Y, Ha CS (2008) Polymers for flexible displays: from material selection to device applications. Prog Polym Sci 33:581–630. doi:10.1016/j.progpolymsci.2007.11.004
5. Hildebrand HF, Blanchemain N, Mayer G, Chai F, Lefebvre M, Boschin F (2006) Surface coatings for biological activation and functionalization of medical devices. Surf Coat Technol 200:6318–6324. doi:10.1016/j.surfcoat.2005.11.086
6. Senkevich JJ, Wiegand CJ, Yang GR, Lu TM (2004) Selective deposition of ultrathin poly(p-xylene) films on dielectrics versus copper surfaces. Chem Vap Deposition 10:247–249. doi:10.1002/cvde.200304179
7. Vaeth KM, Jensen KF (2000) Transition metals for selective chemical vapor deposition of parylene-based polymers. Chem Mater 12:1305–1313. doi:10.1021/cm990642p
8. Chen HY, Lai JH, Jiang X, Lahann J (2008) Substrate-selective chemical vapor deposition of reactive polymer coatings. Adv Mater 20:3474–3408. doi:10.1002/adma.200800455
9. Stoliarov SI, Westmoreland PR, Nyden MR, Forneyb GP (2003) A reactive molecular dynamics model of thermal decomposition in polymers: I. Poly(methyl methacrylate). Polymer 44:883–894. doi:10.1016/S0032-3861(02)00761-9
10. Stewart JJP (2007) Optimization of parameters for semiempirical methods V: modification of NDDO approximations and application to 70 elements. J Mol Model 13:1173–1213. doi:10.1007/s00894-007-0233-4
11. Frenklach M, Carmer CS (1999) Molecular Dynamics using combined quantum and empirical forces: applications to surface reactions. Adv Classical Trajectory Methods 4:27–63
12. Vasenkov AV, Sengupta D, Frenklach M (2009) Multiscale modeling catalytic decomposition of hydrocarbons during carbon nanotube growth. J Phys Chem B 113:1877–1882. doi:10.1021/jp808346h
13. Stewart JJP (1990) Semiempirical molecular orbital methods. In: Lipkowitz KB, Boyd DB (eds) Reviews in Computational Chemistry. VCH, New York, pp 45–81. doi:10.1002/9780470125786.ch2
14. Pamur HO, Halicio lu T (1976) Evaluation of morse parameters for metals. Phys Stat Sol A 37:695–699. doi:10.1002/pssa.2210370242
15. Beeman J (1976) Some multistep methods for use in molecular dynamics calculations. J Comput Phys 20:130–139. doi:10.1016/0021-9991(76)90059-0
16. Berendsen HJC, Postma JPM, van Gunsteren WF, DiNola A, Haak JR (1984) Molecular-Dynamics with coupling to an external bath. J Chem Phys 81:3684–3690. doi:10.1063/1.448118
17. Puddephatt RJ (1979) Gold chemistry today. Endeavour 3:78–81. doi:10.1016/0160-9327(79)90070-X
18. Thompson SJ, Lewis SP (2006) Revisiting the (110) surface structure of TiO_2: a theoretical analysis. Phys Rev B 73:073403(1-4). doi:10.1103/PhysRevB.73.073403
19. Schmidbaur H (ed) (1999) Gold: progress in chemistry, biochemistry and technology. Wiley, Chichester, pp 349–427
20. Schmidbaur H (2000) The aurophilicity phenomenon: a decade of experimental findings, theoretical concepts and emerging applications. Gold Bull 33:3–10
21. Stewart JJP (2008) Application of the PM6 method to modeling the solid state. J Mol Model 14:499–535. doi:10.1007/s00894-008-0299-7
22. Kahouli A, Sylvestre A, Ortega L, Jomni F, Yangui B, Maillard M, Berge B, Robert JC, Legrand J (2009) Structural and dielectric study of parylene C thin films. Appl Phys Lett 94:152901(1–3) doi:10.1063/1.3114404
23. Wu H (1999) Chemical property calculation through JavaScript and applications in QSAR. Molecules 4:16–27. doi:10.3390/40100016
24. Beard RB, Hung BN, Schmukler R (1992) Biocompatibility considerations at stimulating electrode interfaces. Ann Biomed Eng 20:395–410. doi:10.1007/BF02368539
25. Lyon JT, Andrews L (2006) Electron deficient carbon-titanium triple bonds: formation of triplet XC/TiX3 methylidyne complexes. Inorg Chem 45:9858–9863. doi:10.1021/ic0610379
26. Vastine BA, Hall MB (2009) The molecular and electronic structure of carbon–hydrogen bond activation and transition metal assisted hydrogen transfer. Coord Chem Rev 253:1202–1218. doi:10.1016/j.ccr.2008.07.015
27. Fanelli AJ, Maeland AJ, Rosan AM, Crissey RK (1985) Use of hydride-forming metals as renewable chemical reagents: the dehydrogenation of isobutane to isobutene. J Chem Soc Chem Commun 1:8–10
28. Perutza RN, Braunb T (2006) Transition metal-mediated C–F bond activation. In: Mingos DMP, Parkin G (eds) Comprehensive organometallic chemistry III: from fundamentals to applications. Elsevier, Dordrecht, pp 725–758
29. Charlton G, Howes PB, Nicklin CL, Steadman P, Taylor JSG, Muryn CA, Harte SP, Mercer J, McGrath R, Norman D, Turner TS, Thornton G (1997) Relaxation of TiO_2(110)-(1×1) using surface X-ray diffraction. Phys Rev Lett 78:495–498. doi:10.1103/PhysRevLett.78.495
30. Lindsay R, Wander A, Ernst A, Montanari B, Thornton G, Harrison NM (2005) Revisiting the surface structure of TiO_2(110): a quantitative low-energy electron diffraction study. Phys Rev Lett 94:246102(1–4). doi:10.1103/PhysRevLett.94.246102